Published in final edited form as:
Biochemistry. 2009 June 30; 48(25): 6002–6011. doi:10.1021/bi900602h.

Pseudo-hyperphosphorylation causing AD-like changes in tau has significant effects on its polymerization†

Qian Sun and **T. Chris Gamblin***
Department of Molecular Biosciences, University of Kansas, Lawrence, KS 66045

Abstract

The microtubule-associated protein tau, in a hyperphosphorylated form, aggregates into insoluble paired-helical filaments (PHFs) in Alzheimer's disease (AD) and other tauopathies. In AD, there are approximately 8 mol of phosphate per mol of tau distributed among approximately 30 PHF phosphorylation sites as compared to 2–3 phosphate per mol in normal brain. In AD, kinases such as glycogen synthase kinase-3β (GSK-3β) are believed to be involved in generation of hyperphosphorylated tau. However, the functional consequences of hyperphosphorylation on the microtubule binding and polymerization of tau are not well understood. To address this question, we have generated pseudo-hyperphosphorylation mutants consisting of six and seven sites in the proline rich region and carboxy-terminus of tau by amino acid substitution. In addition, several single, double and triple pseudo-phosphorylation mutants were also generated. Pseudo-phosphorylation of tau decreases its affinity for microtubules, and pseudo-hyperphosphorylated forms of tau do not have significantly decreased microtubule binding as compared to single and double-sites. Three pseudo-hyperphosphorylated forms of tau with altered SDS-PAGE migration have a greater effect on its inducer mediated polymerization, slowing the rate of nucleation and elongation. Based on the observations that pseudo-hyperphosphorylated tau has decreased affinity for microtubules and reduced inducer-initiated rates of nucleation and polymerization, we propose that this combination could be the cause for the increased cytotoxicity of hyperphosphorylated tau in Alzheimer's disease and also explain the potentially beneficial role of tau polymerization and NFT formation.

Neurofibrillary tangles (NFTs) are a prominent hallmark of Alzheimer's disease (AD) and other related neurodegenerative disorders, such as frontotemporal dementia and Parkinsonism linked to chromosome 17 (FTDP-17) (reviewed in (*1*)). Although the role of NFTs in Alzheimer's disease is not clear, the location and amount of NFTs directly correlate with the type and severity of cognitive impairment (2,3). NFTs contain large amounts of abnormal protein deposits in the form of straight and paired-helical filaments (4,5) that are composed almost entirely of the microtubule-associated protein tau (6–9) in a hyperphosphorylated state (6). Tau protein is a soluble protein that normally functions to promote the assembly and stabilization of the microtubule cytoskeleton (10), and phosphorylation of tau is known to alter its functions (reviewed in (11)). However, it is still unclear how tau hyperphosphorylation is linked to its aggregation and neuronal degeneration observed in these diseases.

At least 30 phosphorylation sites in PHF tau, about half of which are proline-directed sites, have been identified by mass spectrometry and phospho-amino acid analysis or by phosphorylation-specific monoclonal antibodies. (reviewed in (11,12)). The kinase(s) responsible for the hyperphosphorylation of tau in AD is not clear. It has been suggested that

†Support was provided by NIH AG022428 (TCG) and NIH AG025898 (TCG).

*Address correspondence and reprint requests to: T. Chris Gamblin, Department of Molecular Biosciences, University of Kansas, 1200 Sunnyside Avenue, Lawrence, KS 66045, Tel: 785-864-5065, Fax: 785-864-5321, e-mail: gamblin@ku.edu.

more than one combination of kinases and/or phospatases might be involved in converting normal tau to hyperphosphorylated tau (13). The proline-directed kinase GSK-3β is believed to be involved in this process since it phosphorylates tau at many of the same sites that are found to be phosphorylated in paired helical filaments of AD (14–17), and active GSK-3β is associated with the development of NFTs in AD (18). According to our previous observations, GSK-3β phosphorylates soluble and polymerized tau at a minimum of eleven and five sites respectively (19,20). Phosphorylation at these sites does not change the amount of tau polymerization, but is sufficient to cause tau filaments to coalesce into tangle-like aggregates similar to those isolated from Alzheimer's disease brain (19,20).

Due to the number and proximity of tau phosphorylation, in combination with the relative promiscuity with which most kinases act upon tau, the use of kinases to investigate the effects of specific sites on the function of tau is virtually impossible. It is therefore common for these investigations to employ site-directed mutagenesis to generate pseudo-phosphorylation variants of tau (21–28), although this approach is unlikely to completely mimic phosphorylative changes. We previously showed that the amino acid substitution of glutamic acid for serines or threonines to generate pseudo-phosphorylation mutations at S202 and T205 resulted in only subtle effects on the polymerization characteristics and microtubule binding of tau (28). However, it is not known whether adding additional pseudo-phosphorylation sites that are normally phosphorylated by GSK-3β to generate a "pseudo-hyperphosphorylation" version of tau has a greater effect on its function. To address this question, we have generated pseudo-hyperphosphorylated variants with six (6-phos) and seven (7-phos) pseudo-phosphorylation changes. The sites chosen for investigation include the five sites that are phosphorylated by GSK-3β when tau is in a polymerized state (S199, T205, T231, S396 and S404) (20). 6-phos also included pseudo-phosphorylation at S202. S202 was added to the core five sites since the AT8 antibody recognizes phosphorylation of tau at both S199 and S202 (29), and antibodies to S202 alone were not available for our previous study of GSK3β phosphorylation of tau. Similarly, S235, which is recognized in combination with T231 by the TG-3 antibody (30), was added to 6-phos to generate a 7-phos mutant. Single, double and triple pseudo-phosphorylation mutants were also investigated to control for the possibility that fewer sites could have similar effects to the pseudo-hyperphosphorylated versions of tau. In addition to S199, S202, T205, T231, S235, S396 and S404, other sites were also investigated. T212E was included since it has previously be shown to promote the in vitro assembly of tau to a high level (26). S208D, S210D and S208/210D were also included. These sites are not phosphorylated by GSK-3β, but are in the same proline-rich region of tau that the majority of GSK-3β phosphorylation sites are found. They are known to be phosphorylated by tau-tubulin kinase (TTK) (31) and are also phosphorylated in PHF tau (32). The pseudo-phosphorylation mutants were assayed for changes in SDS-PAGE migration, microtubule binding and arachidonic acid-induced polymerization. We have made two key observations: most pseudo-phosphorylation and pseudo-hyperphosphorylation variants decrease the microtubule binding of tau in a fashion similar to GSK-3β phosphorylated tau, and kinetic analyses of polymerization indicate that pseudo-hyperphosphorylated tau mimics with AD-like changes in SDS-PAGE electrophoretic mobility have increased lag times and reduced apparent rates of elongation compared to single or paired mimics. These results suggest a possible mechanism for the increased toxicity of hyperphosphorylated tau in vivo.

Materials and Methods

Chemicals and Reagents

Arachidonic acid was obtained from Cayman Chemicals (Ann Arbor, MI), IPTG from Calbiochem (EMD Biosciences, La Jolla, CA), SDS-PAGE protein marker from Invitrogen (Gaithersburg, MD), urea from Bio-Rad (Hercules, CA), and uranyl acetate and formvar carbon

coated grids from Electron Microscopy Sciences (Hatfield, PA). Wild-type, P301L and pseudo-phosphorylation mutant tau protein (441 amino acids) were expressed and purified as described previously (28). Pseudo-phosphorylation mutants were generated using the QuikChange site-directed mutagenesis kit from Stratagene (La Jolla, CA). S/T to E mutants and S/T to D mutants were generated at amino acids S199 and T231. S199E was found to have indistinguishable polymerization characteristics as S199D (not shown). T231E and T231D were also indistinguishable in their polymerization (not shown). Protein concentration was determined by a commercial BCA assay from Pierce Chemical (Rockford, IL) using bovine serum albumin (Pierce Chemical, Rockford, IL) as a standard.

SDS-PAGE and SDS-PAGE with urea

Protein samples (1 μg per lane) were boiled for 5 min in sample buffer containing 2% SDS and 1% beta-mercapto-ethanol, fractionated on 15% SDS-PAGE and stained with Coomassie brilliant blue (33). For denaturing SDS-PAGE, protein samples (1 μg per lane) were boiled for 5 min in sample buffer containing 2% SDS and 1% beta-mercapto-ethanol and 6 M urea. Samples were fractionated on 15% SDS-PAGE with 6 M urea and stained with Coomassie brilliant blue (33).

Kinetics of ARA induced polymerization

2 μM tau protein (wild-type and pseudo-phosphorylation tau mutants) was incubated in polymerization buffer (10 mM HEPES pH 7.64, 100 mM NaCl, 0.1 mM EDTA and 5 mM DTT) at room temperature in the presence of 75 μM arachidonic acid (ARA) (in ethanol, final concentration: 3.75%) in the 5 × 5 mm optical glass fluorometer cuvettes (Starna Cells, Atascadero, CA) (34). The amount of polymerization was monitored by LLS at regular intervals for 20 hr with 5 mW solid state laser (λ= 475 nm, B & W Tek, Inc., Newark, DE). Images were captured at a right angle to the incident light using a SONY XC-ST270 digital camera. Captured images were imported into Adobe Photoshop 7.0.1 and the intensity of the scattered light was measured as described previously (28). The pictures were captured at an aperture of f5.6–8 or f8 and then normalized to the intensity corresponded to the exposure at f5.6–8. The data were fit to a non-linear Gompertz function:

$$y=ae^{-e^{-\left(\frac{(t-t_i)}{b}\right)}},$$

where y is the value of laser light scattering measured at time *t*; a is the maximum amount of light scattering; t_i is the point of inflection where the increase in scattering is at its maximum; and *b* is equal to $1/k_{app}$. k_{app} is proportional to the rate of polymerization (26). The lag time for polymerization, or the amount of time required to observe significant amounts of polymerization, was calculated using the formula: $t_i - b$ (26). The Gompertz function has been used as a model for growth curves (35), including as a model for tau polymerization (26). Errors in the kinetics parameters were assessed by individually fitting three separate kinetics experiments to the Gompertz function to obtain three independent measures of LLS_{max}, k_{app} and lag times. These values were averaged and reported ± standard deviation.

Transmission electron microscopy

Tau polymerization reactions were diluted 10-fold with polymerization buffer then fixed with glutaraldehyde (2% final concentration) for 5 min. Ten microliters of fixed reactions were placed on formvar-carbon coated grids (1 min), washed with water, blotted, washed with 2% uranyl acetate, blotted, stained with 2% uranyl acetate (1 min), then blotted dry. Grids were viewed with a TECNAI G^2 20 electron microscope (FEI Company, Hillsboro, OR) and digital images were captured with the Gatan Digital Micrograph imaging system.

Microtubule binding assay

The microtubule binding assay was performed in general tubulin buffer (80 mM PIPES, pH 7, 1 mM $MgCl_2$, 1 mM EGTA). Tau protein ranging from 0.125 μM to 10 μM were mixed with paclitaxel stabilized microtubules at a final concentration of 1.62 μM tubulin dimer in a 50 μL reaction. Samples were incubated at room temperature for 30 min, and centrifuged in a Beckman Optima TLX ultracentrifuge at 100,000 × g for 5 min to sediment the microtubules and tau bound to the microtubules. The pellets were resuspended in SDS sample buffer and microtubules were separated from tau bound to microtubules by SDS-PAGE. The concentration of tau bound to the microtubules was determined by the intensity of tau band by Adobe Photoshop and normalized to the intensity of tubulin band. The tau band was normalized to the intensity of the tubulin bands in each lane to account for any differences in centrifugation or resuspension of samples because the amount of tubulin should be constant in all binding reactions. The amount of free tau was determined by subtracting the amount of bound tau from the total amount of tau. The concentration of bound tau were plotted versus the concentration of free tau in GraphPad Prism and fit to a one site binding (hyperbola) equation.

Results

Selection and generation of pseudo-phosphorylation mutants

Hyperphosphorylated tau in Alzheimer's disease (AD) is phosphorylated at a molar ratio of approximately 5–9 mol phosphate per mol of tau whereas normal tau contains only 2–3 mol phosphate per mol of tau (36). However, the role of this hyperphosphorylation is poorly understood. To better understand the effects of tau hyperphosphorylation, pseudo-phosphorylation mutants were constructed. We chose to focus on the five sites known to be phosphorylated by GSK-3β in vitro when arachidonic acid-induced tau filaments are used as the substrate (S199, T205, T231, S396 and S404) (20). Pseudo-phosphorylation changes at S202 were added to generate the 6-phos, and both S202 and S235 were added to generate 7-phos (Figure 1A). These sites were included since S202 is often found phosphorylated along with S199, and S235 is often found phosphorylated along with T231. Single, paired and triplet mutants were investigated to determine whether fewer sites might also have an effect on the function of tau (Figure 1A). We also investigated a GSK-3β site in the same proline rich region but not among the sites above (T212) as a control. As further controls, non-proline directed sites S208, S210 and S208/S210 were investigated. The disease causing P301L tau mutation was included in the analyses as a positive control.

Pseudo-phosphorylation at S199/S202/T205, S396/S404, 6-Phos and 7-Phos induces AD-like changes in electrophoretic mobility

Alzheimer's disease hyperphosphorylated tau and recombinant tau phosphorylated by GSK-3β in vitro have an upward band shift when analyzed by SDS-PAGE (19,37). This upward band shift is the definitive characteristic of hyperphosphorylated tau in neurodegenerative disorders (1). To determine whether the pseudo-phosphorylation mutants can cause this upward band shift, the pseudo-phosphorylation forms of tau were analyzed by coomassie-stained SDS-PAGE electrophoresis. S199/S202/T205E, S396/S404E, 6-Phos and 7-Phos had an upward shift in mobility compared to wild-type tau (Figure 1B). The apparent molecular masses for wild-type, S199/S202/T205E, S396/S404E, 6-Phos and 7-Phos were 70 kDa, 72 kDa, 75 kDa, 78 kDa and 78 kDa, respectively. P301L tau and all other pseudo-phosphorylation mutants did not show a change in mobility (data not shown). The mobility shift of pseudo-phosphorylation mutants was reduced in the presence of 6M urea (molecular weights for wild-type, S199/S202/T205E, S396/S404E, 6-Phos and 7-Phos were 70 kDa, 70 kDa, 71 kDa, 72 kDa and 72 kDa, respectively, Figure 1C). This phenomenon of altered mobility in SDS that is abolished in urea has been described in the literature as a SDS-resistant change in conformation (33,38–41). Because S199/S202/T205E, S396/S404E, 6-Phos and 7-Phos all demonstrated an AD-like shift

in mobility as a result of phosphorylation-like changes, we conclude that they have the characteristics of hyperphosphorylated tau. These mutants will therefore be referred to as pseudo-hyperphosphorylated tau throughout the manuscript.

Pseudo-phosphorylation of tau changes its affinity for microtubules

Because FTDP-17 mutations (42) and pseudo-phosphorylation mutations (28) in tau can alter its interactions with microtubules, we measured the microtubule binding affinity of P301L tau and fifteen pseudo-phosphorylation mutants using a centrifugation assay (43). Pellets containing microtubules and bound tau were resuspended in SDS-sample buffer and analyzed by coomassie-stained SDS-PAGE (Figure 2A). The concentration of tau bound to the microtubules was determined by the intensity of tau band and normalized to the intensity of tubulin band (Figure 2A). Normalization of the amount of tau relative to tubulin was performed to take into account any differences in sedimentation or resuspension of the pellets. The concentration of free tau was calculated by subtracting the measured bound tau from the total tau added to the reaction. The amount of bound tau was plotted against free tau. Two representative curves (wild-type tau and 7-Phos) are shown in Figure 2B. The data were fit to a simple one-site binding equation to determine the affinity of binding (K_d) and the maximal amount of bound tau (B_{max}) (Figure 2C and 2D). All proteins examined, with the exception of S199E, S202E and S208D, had significantly lower affinities for microtubules than was observed with wild-type tau (Figure 2B). The decreases in binding affinity were all in the 2–3 fold reduction range, which is in general agreement with previously published reports of GSK-3β phosphorylation of tau (44) and the P301L mutation (42). The stoichiometry of binding to microtubules was not greatly affected (Figure 2C).

Pseudo-phosphorylation influences the arachidonic acid induction of tau polymerization

To determine whether pseudo-phosphorylation mutations of tau have an effect on the arachidonic acid (ARA) induction of tau polymerization, each protein at a final concentration of 2 μM was incubated in the presence of 75 μM ARA. This protein to inducer ratio was chosen since it has been shown to be the optimal condition for the arachidonic acid induction of wild-type tau polymerization (34). The kinetics of polymerization of each mutant were followed by right angle laser light scattering and compared to wild-type tau. Representative curves are shown in Figure 3A. The data were fit to a Gompertz function to determine the maximal amount of light scattering (LLS_{max}) (Figure 3B), the apparent proportional growth rate (k_{app},Figure 3C), and the lag time of polymerization (Figure 3D). No significant increases in polymerization were observed for the pseudo-phosphorylation mutants (Figure 3B), although the FTDP-17 mutation P301L did have a significant increase in the extent of polymerization compared to wild-type, as expected (45). Several pseudo-phosphorylation variants (S202/T205E, S199/S202/T205E, S208/S210D, T231E, S396/S404E, 6-Phos and 7-Phos) had significantly less maximal polymerization as compared to wild-type.

The apparent proportional growth rate, k_{app}, was not significantly altered for most of the mutants (Figure 3C). The FTDP-17 mutation P301L has been shown to have the most dramatic effects in increasing the apparent rate of polymerization as compared to wild-type tau protein (45), and had a significantly greater k_{app} than wild-type tau and all the pseudo-phosphorylation mutants. Mutants S210D and T231D also had significantly greater k_{app} values than wild type, but still less than P301L tau (Figure 3C). S199/S202/T205E, 6-phos and 7-phos all had significantly lower k_{app} than wild type tau (Figure 3C).

Nucleation-elongation polymerization pathways are also typically characterized by a lag time in the polymerization process. Wild type tau had a lag time of 19 minutes (Figure 3D). P301L tau had a significantly reduced lag time, as expected (45). S210D, S208/S210D, T231E and T231E/S235D also had significantly reduced lag times, but greater than P301L tau (Figure

3D). 6-phos had a significantly longer lag time than wild type tau (Figure 3D). On average, S199/S202/T205E and 7-Phos had longer lag times than wild type, but these differences did not reach statistical significance (Figure 3D).

Pseudo-phosphorylation changes the morphology of ARA-induced tau filaments

To determine whether filament morphology (number and length of filaments) was changed by pseudo-phosphorylation, samples from polymerization reactions were prepared and viewed by TEM (Figure 4). Filaments from six fields of view were combined into a single data set and then ranked according to their length (examples are shown Figure 5A). Particles less than 15nm in their longest dimension were not included in the analysis because particles smaller than this cutoff value are smaller than the average filament width of arachidonic acid induced filaments (19), and therefore difficult to distinguish from background. In general, pseudo-phosphorylation mutants tended to form fewer but longer filaments than wild-type tau (Figure 5B and 5C). The standard deviation of the average lengths was roughly equal to the value of the average lengths for most proteins, as is expected for exponentially distributed data (46). The standard error of the mean is also shown, as this is an estimate of the accuracy of the determination of the true mean. Among these mutants, the three with the most phosphorylation sites formed the longest filaments (S199/S202/T20E5, 6-Phos and 7-Phos) (Figure 5C). However, the overall amount of filament formation observed in six fields was relatively similar for most all proteins (Figure 5D), with the possible exceptions of T231E, S202/T205E, T205E and S396/404E which seemed to have somewhat reduced levels of polymerization compared to the other proteins (Figure 5D). In general, pseudo-phosphorylation of tau resulted in fewer, but longer filaments as compared to wild-type (Figure 4 and 5). In contrast, the rapidly polymerizing P301L formed more, but shorter filaments than wild-type tau, resulting in an overall increase in the amount of polymerized material (Figure 5A–D).

Quantitative analysis of differences between the filaments is difficult due to the differences in the number of filaments, the variability in filament distribution on the TEM grid, the biological variability in filament lengths, and the exponential distribution of filament lengths. Therefore, it is possible that the apparent differences in filament length distributions (Figure 5) could be due to differences in sampling. We therefore measured 500 filaments for each mutant and determined the number-average length ($L_n=(\Sigma N_i L_i)/(\Sigma N_i)$, Figure 6) for each mutant (47). With the exception of T231, all pseudo-phosphorylation mutants had greater average filament lengths than wild type protein. This analysis also confirmed that S199/S202/T205E, 6-Phos and 7-Phos had the greatest tendencies for forming long filaments.

Discussion

Significance of pseudo-phosphorylation mutants sites

Hyperphosphorylation of the microtubule-associated protein tau is a pathological hallmark of Alzheimer's disease and other tauopathies. Many kinases have been shown to be involved in this phosphorylation process, and GSK-3β is believed to be a major contributor to tau/PHF phosphorylation (reviewed in (11)). In previous studies, we found that GSK-3β phosphorylation of pre-formed tau filaments at sites including S199, T205, T231, S396 and S404 can cause tau filaments to coalesce into NFT-like structures (20). Because these five sites are recognized by specific AD-associated antibodies, we sought to test whether pseudo-phosphorylation at these sites would have an impact on the function of tau (summarized in Table 1).

Role of phosphorylation in tau polymerization

Phosphorylation of tau at specific sites has been suggested to correlate with the formation of neurofibrillary tangles (NFTs), raising the possibility that a major function of tau

phosphorylation is to promote tau polymerization (48). Under conditions that we have determined to be optimal for wild-type tau polymerization (34), pseudo-phosphorylation of tau mildly reduced its polymerization, which is consistent with previously published reports using in vitro GSK-3β phosphorylated tau (19,49). The kinetics of polymerization for most of the single and double phosphorylation variants were not significantly changed (Table 1). However, the pseudo-hyperphosphorylated version of tau (S199/S202/T205E, 6-Phos and 7-Phos) had a drastically decreased rate of elongation and a pronounced lag time. This suggests a deficiency in the nucleation step for the pseudo-hyperphosphorylation mimics. The observation of fewer but longer filaments with pseudo-hyperphosphorylation mutants agree with this idea.

The effect on filament nucleation and filament length was greatest with the "pseudo-hyperphosphorylated" versions of tau. 6-phos and 7-phos were generated from the combination of multiple pseudo-phosphorylation sites in both the proline-rich and C-terminal regions of tau. The effects on polymerization of 6-phos and 7-phos seem to be greater than those observed by the heparin (49) or arachidonic acid (19) induction of GSK-3β phosphorylated tau polymerization. However, GSK-3β phosphorylation in vitro only results in 2–4 mol phosphate incorporation per mol of tau distributed unequally over as many as fourteen sites (19,20,49–51). 6-phos and 7-phos are homogeneous in their modifications and therefore are more highly modified than the average GSK-3β phosphorylated tau protein.

Our previous studies have shown that the presence of arachidonic acid drastically reduces the energetic barrier for the nucleation of polymerization (34). The observation that pseudo-hyperphosphorylation mutants are less likely to nucleate could be explained by diminished interactions with arachidonic acid as a result of altered conformations of the proteins conferred by pseudo-phosphorylation. In support of this, the pseudo-hyperphosphorylated proteins had altered SDS-PAGE electrophoretic mobility that was abolished in the presence of urea. This phenomenon has been described as an SDS-resistant change in conformation of tau (33,38–41), and indicates that pseudo-phosphorylated proteins could interact differently with SDS or with arachidonic acid.

It should be mentioned that a previous report found that pseudo-phosphorylation of tau at several sites (including S199, S199/S202/T205 and T212) enhanced polymerization by 2–3 fold over non-modified tau (26). We obtain similar results when using concentrations of arachidonic acid that inhibit wild type tau polymerization (125–150 μM, data not shown). It is not clear whether these results at high inducer to protein ratios have physiological relevance, but they are consistent with the hypothesis that pseudo-phosphorylation of tau can decrease its interactions with arachidonic acid.

Role of phosphorylation in microtubule binding

Most pseudo-phosphorylation forms of tau significantly decreased microtubule binding by 2–3 fold without significantly changing the saturation levels (Table 1), which agrees with previous studies investigating the effects of tau phosphorylation at proline-directed phosphorylation sites (49). However, results from multiple site constructs were not consistently additive. For example, both T231E and S235D had lower affinities than wild-type for microtubules. However, the T231E/S235D double mutant had an affinity similar to the individual mutations. And while S202/T205E had a lower affinity for microtubules than the individual mutants, the addition of S199E to form S199/S202/T205E actually improved microtubule binding (albeit at a lower affinity than wild-type tau). The constructs with six or seven pseudo-phosphorylation sites did not show dramatically different levels of microtubule binding than single or double mutants. We conclude that microtubule binding is regulated in a complicated site-specific fashion, and the levels of phosphorylation are less of a determinant of microtubule binding than the actual sites involved.

Phosphorylation, polymerization, NFTs and toxicity

Since the establishment of the correlation between the number of NFTs with the degree of dementia in AD, NFTs have been widely accepted as a toxic species in AD (reviewed in (52)). However, recent observations in tau-expressing cultured cell, transgenic Drosophila and mouse models suggest that the toxicity is independent of NFT formation and NFTs may form as a result of cellular attempts to reduce toxicity (reviewed in (53)). NFTs contain large amounts of abnormal hyperphosphorylated tau (6) in the form of straight and paired-helical filaments (4,5). The abnormal hyperphosphorylation of tau is one of the post-translational modifications of tau known to be related to toxicity, filament formation and the formation of NFTs (reviewed in (54)). The apparent phosphorylation-dependent toxicity of tau could be due to the disruption of microtubule dynamics through sequestration of normal tau (55–57), and could be reduced through the polymerization of phosphorylated tau (58). Additionally, the presence of soluble hyperphosphorylated tau is correlated with cognitive deficiencies in a transgenic mouse model (59). These results suggest that tau aggregation could protect against phosphorylation-induced microtubule disruption and subsequent neurodegeneration.

Our results provide a potential biochemical mechanism for the potential cytotoxicity of hyperphosphorylated tau. Phosphorylated tau binds to microtubules less tightly, so that there would be an increase in cytoplasmic tau and increased microtubule instability. It has also been shown through other work that hyperphosphorylated tau may sequester normal tau (56), further disrupting microtubule dynamics. Pseudo-hyperphosphorylated tau also has a decreased rate of polymerization, potentially increasing the amount of time it is soluble in the cytoplasm where it could sequester normal tau. It is also possible that the fibrillization of abnormally phosphorylated tau could protect cells from toxic effects. We have previously shown tau phosphorylation by GSK-3β is sufficient to induce the bundling tau filaments into NFT-like structures in a cell-free in vitro system (20). These observations are consistent with data from transgenic mouse models showing that NFT formation is not necessarily the toxic element of neurodegeneration and may instead play a protective role (59–61).

Acknowledgments

We thank Carolyn Rankin and Kellen Voss for critical reading of the manuscript. We also thank Mike Branden for protein production. This work was supported by NIH AG022428 (TCG) and NIH AG025898 (TCG).

Abbreviations

AD
: Alzheimer’s disease

GSK-3β
: glycogen synthase kinase-3β

TTK
: tau-tubulin kinase

NFTs
: neurofibrillary tangles

FTDP-17
: frontotemporal dementia and Parkinsonism linked to chromosome 17

ARA
: arachidonic acid

LLS

laser light scattering

References

1. Sergeant N, Delacourte A, Buee L. Tau protein as a differential biomarker of tauopathies. Biochim Biophys Acta 2005;1739:179–197. [PubMed: 15615637]
2. Arriagada PV, Growdon JH, Hedley-Whyte ET, Hyman BT. Neurofibrillary tangles but not senile plaques parallel duration and severity of Alzheimer's disease. Neurology 1992;42:631–639. [PubMed: 1549228]
3. McKee AC, Kosik KS, Kowall NW. Neuritic pathology and dementia in Alzheimer's disease. Ann Neurol 1991;30:156–165. [PubMed: 1910274]
4. Kidd M. Paired helical filaments in electron microscopy of Alzheimer's disease. Nature 1963;197:192–193. [PubMed: 14032480]
5. Yagishita S, Itoh Y, Nan W, Amano N. Reappraisal of the fine structure of Alzheimer's neurofibrillary tangles. Acta Neuropathol 1981;54:239–246. [PubMed: 7257733]
6. Grundke-Iqbal I, Iqbal K, Tung YC, Quinlan M, Wisniewski HM, Binder LI. Abnormal phosphorylation of the microtubule-associated protein tau (tau) in Alzheimer cytoskeletal pathology. Proc Natl Acad Sci U S A 1986;83:4913–4917. [PubMed: 3088567]
7. Kondo J, Honda T, Mori H, Hamada Y, Miura R, Ogawara M, Ihara Y. The carboxyl third of tau is tightly bound to paired helical filaments. Neuron 1988;1:827–834. [PubMed: 2483105]
8. Kosik KS, Joachim CL, Selkoe DJ. Microtubule-associated protein tau (tau) is a major antigenic component of paired helical filaments in Alzheimer disease. Proc Natl Acad Sci U S A 1986;83:4044–4048. [PubMed: 2424016]
9. Wischik CM, Novak M, Thogersen HC, Edwards PC, Runswick MJ, Jakes R, Walker JE, Milstein C, Roth M, Klug A. Isolation of a fragment of tau derived from the core of the paired helical filament of Alzheimer disease. Proc Natl Acad Sci U S A 1988;85:4506–4510. [PubMed: 3132715]
10. Weingarten MD, Lockwood AH, Hwo SY, Kirschner MW. A protein factor essential for microtubule assembly. Proc Natl Acad Sci U S A 1975;72:1858–1862. [PubMed: 1057175]
11. Stoothoff WH, Johnson GV. Tau phosphorylation: physiological and pathological consequences. Biochim Biophys Acta 2005;1739:280–297. [PubMed: 15615646]
12. Buee L, Bussiere T, Buee-Scherrer V, Delacourte A, Hof PR. Tau protein isoforms, phosphorylation and the role in neurodegenerative disorders. Brain Res Brain Res Rev 2000;33:95–130. [PubMed: 10967355]
13. Wang JZ, Grundke-Iqbal I, Iqbal K. Kinases and phosphatases and tau sites involved in Alzheimer neurofibrillary degeneration. Eur J Neurosci 2007;25:59–68. [PubMed: 17241267]
14. Balaraman Y, Limaye AR, Levey AI, Srinivasan S. Glycogen synthase kinase 3beta and Alzheimer's disease: pathophysiological and therapeutic significance. Cell Mol Life Sci 2006;63:1226–1235. [PubMed: 16568235]
15. Illenberger S, Zheng-Fischhofer Q, Preuss U, Stamer K, Baumann K, Trinczek B, Biernat J, Godemann R, Mandelkow EM, Mandelkow E. The endogenous and cell cycle-dependent phosphorylation of tau protein in living cells: implications for Alzheimer's disease. Mol Biol Cell 1998;9:1495–1512. [PubMed: 9614189]
16. Song JS, Yang SD. Tau protein kinase I/GSK-3 beta/kinase FA in heparin phosphorylates tau on Ser199, Thr231, Ser235, Ser262, Ser369, and Ser400 sites phosphorylated in Alzheimer disease brain. J Protein Chem 1995;14:95–105. [PubMed: 7786411]
17. Wang JZ, Wu Q, Smith A, Grundke-Iqbal I, Iqbal K. Tau is phosphorylated by GSK-3 at several sites found in Alzheimer disease and its biological activity markedly inhibited only after it is prephosphorylated by A-kinase. FEBS Lett 1998;436:28–34. [PubMed: 9771888]
18. Leroy K, Yilmaz Z, Brion JP. Increased level of active GSK-3beta in Alzheimer's disease and accumulation in argyrophilic grains and in neurones at different stages of neurofibrillary degeneration. Neuropathol Appl Neurobiol 2007;33:43–55. [PubMed: 17239007]
19. Rankin CA, Sun Q, Gamblin TC. Tau phosphorylation by GSK-3beta promotes tangle-like filament morphology. Mol Neurodegener 2007;2:12. [PubMed: 17598919]

20. Rankin CA, Sun Q, Gamblin TC. Pre-assembled tau filaments phosphorylated by GSK-3b form large tangle-like structures. Neurobiol Dis 2008;31:368–377. [PubMed: 18588978]
21. Abraha A, Ghoshal N, Gamblin TC, Cryns V, Berry RW, Kuret J, Binder LI. C-terminal inhibition of tau assembly in vitro and in Alzheimer's disease. J Cell Sci 113 Pt 2000;21:3737–3745.
22. Ding H, Matthews TA, Johnson GV. Site-specific phosphorylation and caspase cleavage differentially impact tau-microtubule interactions and tau aggregation. J Biol Chem 2006;281:19107–19114. [PubMed: 16687396]
23. Fath T, Eidenmuller J, Brandt R. Tau-mediated cytotoxicity in a pseudohyperphosphorylation model of Alzheimer's disease. J Neurosci 2002;22:9733–9741. [PubMed: 12427828]
24. Haase C, Stieler JT, Arendt T, Holzer M. Pseudophosphorylation of tau protein alters its ability for self-aggregation. J Neurochem 2004;88:1509–1520. [PubMed: 15009652]
25. Necula M, Chirita CN, Kuret J. Cyanine dye N744 inhibits tau fibrillization by blocking filament extension: implications for the treatment of tauopathic neurodegenerative diseases. Biochemistry 2005;44:10227–10237. [PubMed: 16042400]
26. Necula M, Kuret J. Pseudophosphorylation and glycation of tau protein enhance but do not trigger fibrillization in vitro. J Biol Chem 2004;279:49694–49703. [PubMed: 15364924]
27. Necula M, Kuret J. Site-specific pseudophosphorylation modulates the rate of tau filament dissociation. FEBS Lett 2005;579:1453–1457. [PubMed: 15733856]
28. Rankin CA, Sun Q, Gamblin TC. Pseudo-phosphorylation of tau at Ser202 and Thr205 affects tau filament formation. Brain Res Mol Brain Res. 2005
29. Biernat J, Mandelkow EM, Schroter C, Lichtenberg-Kraag B, Steiner B, Berling B, Meyer H, Mercken M, Vandermeeren A, Goedert M, et al. The switch of tau protein to an Alzheimer-like state includes the phosphorylation of two serine-proline motifs upstream of the microtubule binding region. Embo J 1992;11:1593–1597. [PubMed: 1563356]
30. Jicha GA, Lane E, Vincent I, Otvos L Jr, Hoffmann R, Davies P. A conformation- and phosphorylation-dependent antibody recognizing the paired helical filaments of Alzheimer's disease. J Neurochem 1997;69:2087–2095. [PubMed: 9349554]
31. Tomizawa K, Omori A, Ohtake A, Sato K, Takahashi M. Tau-tubulin kinase phosphorylates tau at Ser-208 and Ser-210, sites found in paired helical filament-tau. FEBS Lett 2001;492:221–227. [PubMed: 11257498]
32. Hanger DP, Betts JC, Loviny TL, Blackstock WP, Anderton BH. New phosphorylation sites identified in hyperphosphorylated tau (paired helical filament-tau) from Alzheimer's disease brain using nanoelectrospray mass spectrometry. J Neurochem 1998;71:2465–2476. [PubMed: 9832145]
33. Eidenmuller J, Fath T, Maas T, Pool M, Sontag E, Brandt R. Phosphorylation-mimicking glutamate clusters in the proline-rich region are sufficient to simulate the functional deficiencies of hyperphosphorylated tau protein. Biochem J 2001;357:759–767. [PubMed: 11463346]
34. Carlson SW, Branden M, Voss K, Sun Q, Rankin CA, Gamblin TC. A complex mechanism for inducer mediated tau polymerization. Biochemistry 2007;46:8838–8849. [PubMed: 17608454]
35. Winsor CP. The Gompertz Curve as a Growth Curve. Proc Natl Acad Sci U S A 1932;18:1–8. [PubMed: 16577417]
36. Kopke E, Tung YC, Shaikh S, Alonso AC, Iqbal K, Grundke-Iqbal I. Microtubule-associated protein tau. Abnormal phosphorylation of a non-paired helical filament pool in Alzheimer disease. J Biol Chem 1993;268:24374–24384. [PubMed: 8226987]
37. Lee VM, Goedert M, Trojanowski JQ. Neurodegenerative tauopathies. Annu Rev Neurosci 2001;24:1121–1159. [PubMed: 11520930]
38. Brandt R, Lee G, Teplow DB, Shalloway D, Abdel-Ghany M. Differential effect of phosphorylation and substrate modulation on tau's ability to promote microtubule growth and nucleation. J Biol Chem 1994;269:11776–11782. [PubMed: 8163474]
39. Eidenmuller J, Fath T, Hellwig A, Reed J, Sontag E, Brandt R. Structural and functional implications of tau hyperphosphorylation: information from phosphorylation-mimicking mutated tau proteins. Biochemistry 2000;39:13166–13175. [PubMed: 11052669]
40. Leger J, Kempf M, Lee G, Brandt R. Conversion of serine to aspartate imitates phosphorylation-induced changes in the structure and function of microtubule-associated protein tau. J Biol Chem 1997;272:8441–8446. [PubMed: 9079670]

41. Litersky JM, Johnson GV. Phosphorylation by cAMP-dependent protein kinase inhibits the degradation of tau by calpain. J Biol Chem 1992;267:1563–1568. [PubMed: 1730702]
42. Hong M, Zhukareva V, Vogelsberg-Ragaglia V, Wszolek Z, Reed L, Miller BI, Geschwind DH, Bird TD, McKeel D, Goate A, Morris JC, Wilhelmsen KC, Schellenberg GD, Trojanowski JQ, Lee VM. Mutation-specific functional impairments in distinct tau isoforms of hereditary FTDP-17. Science 1998;282:1914–1917. [PubMed: 9836646]
43. Vallee RB. A taxol-dependent procedure for the isolation of microtubules and microtubule-associated proteins (MAPs). J Cell Biol 1982;92:435–442. [PubMed: 6120944]
44. Mandelkow EM, Drewes G, Biernat J, Gustke N, Van Lint J, Vandenheede JR, Mandelkow E. Glycogen synthase kinase-3 and the Alzheimer-like state of microtubule-associated protein tau. FEBS Lett 1992;314:315–321. [PubMed: 1334849]
45. Gamblin TC, King ME, Dawson H, Vitek MP, Kuret J, Berry RW, Binder LI. In vitro polymerization of tau protein monitored by laser light scattering: method and application to the study of FTDP-17 mutants. Biochemistry 2000;39:6136–6144. [PubMed: 10821687]
46. Oosawa, F.; Asakura, S. Thermodynamics of the Polymerization of Protein. Academic Press; London; New York: 1975.
47. Janmey PA, Peetermans J, Zaner KS, Stossel TP, Tanaka T. Structure and mobility of actin filaments as measured by quasielastic light scattering, viscometry, and electron microscopy. J Biol Chem 1986;261:8357–8362. [PubMed: 3013849]
48. Augustinack JC, Schneider A, Mandelkow EM, Hyman BT. Specific tau phosphorylation sites correlate with severity of neuronal cytopathology in Alzheimer's disease. Acta Neuropathol (Berl) 2002;103:26–35. [PubMed: 11837744]
49. Schneider A, Biernat J, von Bergen M, Mandelkow E, Mandelkow EM. Phosphorylation that detaches tau protein from microtubules (Ser262, Ser214) also protects it against aggregation into Alzheimer paired helical filaments. Biochemistry 1999;38:3549–3558. [PubMed: 10090741]
50. Connell JW, Gibb GM, Betts JC, Blackstock WP, Gallo J, Lovestone S, Hutton M, Anderton BH. Effects of FTDP-17 mutations on the in vitro phosphorylation of tau by glycogen synthase kinase 3beta identified by mass spectrometry demonstrate certain mutations exert long-range conformational changes. FEBS Lett 2001;493:40–44. [PubMed: 11278002]
51. Reynolds CH, Betts JC, Blackstock WP, Nebreda AR, Anderton BH. Phosphorylation sites on tau identified by nanoelectrospray mass spectrometry: differences in vitro between the mitogen-activated protein kinases ERK2, c-Jun N-terminal kinase and P38, and glycogen synthase kinase-3beta. J Neurochem 2000;74:1587–1595. [PubMed: 10737616]
52. Ballatore C, Lee VM, Trojanowski JQ. Tau-mediated neurodegeneration in Alzheimer's disease and related disorders. Nat Rev Neurosci 2007;8:663–672. [PubMed: 17684513]
53. Rankin CA, Gamblin TC. Assessing the toxicity of tau aggregation. J Alzheimers Dis 2008;14:411–416. [PubMed: 18688091]
54. Iqbal K, Liu F, Gong CX, Alonso AD, Grundke-Iqbal I. Mechanisms of tau-induced neurodegeneration. Acta Neuropathol. 2009
55. Alonso AC, Zaidi T, Grundke-Iqbal I, Iqbal K. Role of abnormally phosphorylated tau in the breakdown of microtubules in Alzheimer disease. Proc Natl Acad Sci U S A 1994;91:5562–5566. [PubMed: 8202528]
56. Alonso AC, Grundke-Iqbal I, Iqbal K. Alzheimer's disease hyperphosphorylated tau sequesters normal tau into tangles of filaments and disassembles microtubules. Nat Med 1996;2:783–787. [PubMed: 8673924]
57. Li B, Chohan MO, Grundke-Iqbal I, Iqbal K. Disruption of microtubule network by Alzheimer abnormally hyperphosphorylated tau. Acta Neuropathol 2007;113:501–511. [PubMed: 17372746]
58. Alonso Adel C, Li B, Grundke-Iqbal I, Iqbal K. Polymerization of hyperphosphorylated tau into filaments eliminates its inhibitory activity. Proc Natl Acad Sci U S A 2006;103:8864–8869. [PubMed: 16735465]
59. Santacruz K, Lewis J, Spires T, Paulson J, Kotilinek L, Ingelsson M, Guimaraes A, DeTure M, Ramsden M, McGowan E, Forster C, Yue M, Orne J, Janus C, Mariash A, Kuskowski M, Hyman B, Hutton M, Ashe KH. Tau suppression in a neurodegenerative mouse model improves memory function. Science 2005;309:476–481. [PubMed: 16020737]

60. Berger Z, Roder H, Hanna A, Carlson A, Rangachari V, Yue M, Wszolek Z, Ashe K, Knight J, Dickson D, Andorfer C, Rosenberry TL, Lewis J, Hutton M, Janus C. Accumulation of pathological tau species and memory loss in a conditional model of tauopathy. J Neurosci 2007;27:3650–3662. [PubMed: 17409229]

61. Spires TL, Orne JD, SantaCruz K, Pitstick R, Carlson GA, Ashe KH, Hyman BT. Region-specific dissociation of neuronal loss and neurofibrillary pathology in a mouse model of tauopathy. Am J Pathol 2006;168:1598–1607. [PubMed: 16651626]

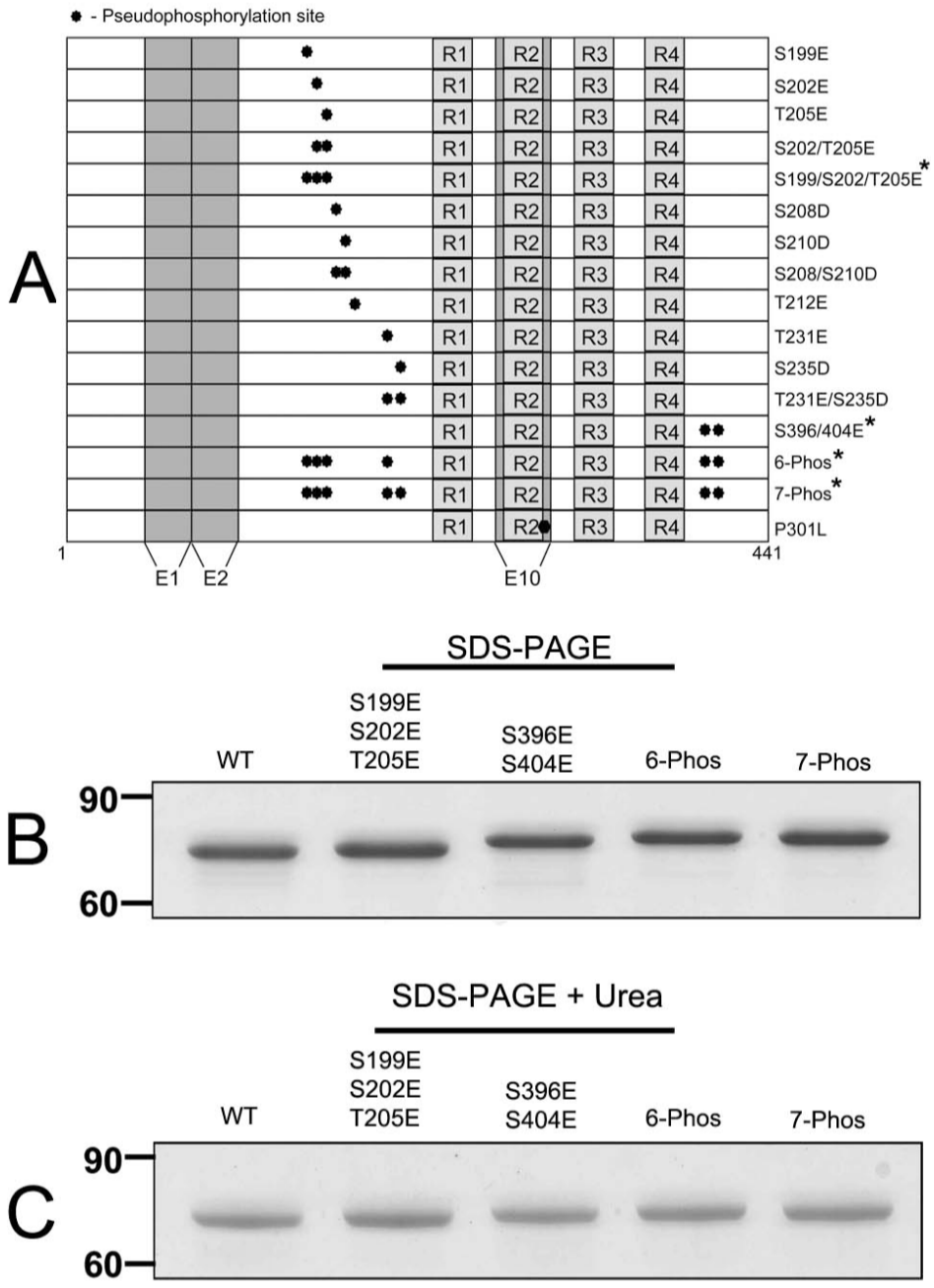

Figure 1. Simulation of phosphorylation by glutamate or aspartate replacement

A) Diagram of phosphorylation sites on full-length tau. Four microtubule binding repeats are indicated by light gray (R1-R4) and exon 2, 3 and 10 are indicated by dark gray boxes. Phosphorylation sites that have been mutated to glutamate or aspartate are indicated to the right of the diagram showing their position. The FTDP-17 mutant, P301L, is also indicated. The mutants with “hyperphosphorylation”-like changes are marked with an asterisk. B) SDS-resistant upward band shifts were observed in the pseudo-phosphorylation mutants S199/S202/T202E, S396/S404E, 6-Phos and 7-Phos. 1 μg tau protein samples (wild-type tau (WT), S199/S202/T202E, S396/S404E, 6-Phos and 7-Phos) were fractionated by SDS-PAGE on a 15% gradient gel. C) SDS-resistant upward band shifts shown by S199/S202/T202E, S396/S404E,

6-Phos and 7-Phos were reduced in the presence of 6M urea. 1 μg tau protein samples (wild-type tau (WT), S199/S202/T205E, S396/404E, 6-Phos and 7-Phos) were fractionated by SDS-PAGE in a 15% gel made with 6M urea.

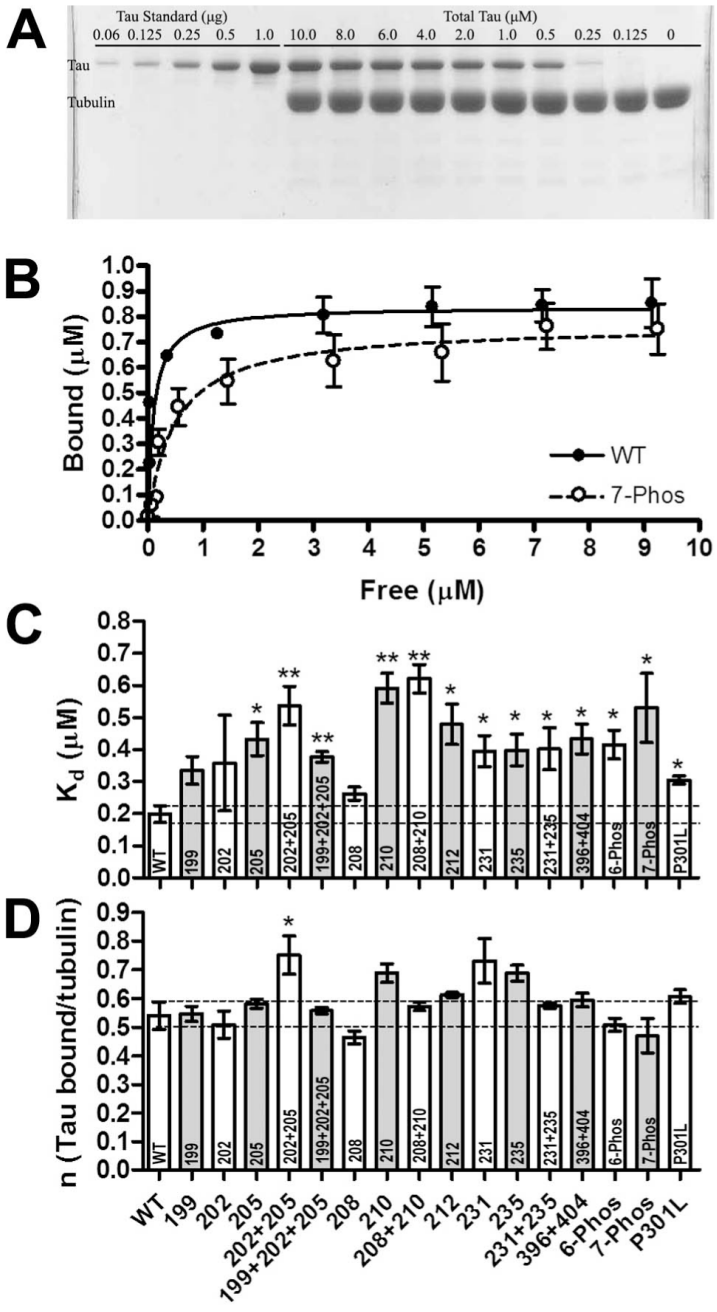

Figure 2. Microtubule binding of pseudo-phosphorylation mutants

The microtubule binding affinities of wild-type and mutant tau were measured using a centrifugal assay to separate bound and unbound tau. A) A representative SDS-PAGE gel after centrifugation. The concentrations of standard tau in first five lanes are 0.06, 0.125, 0.25, 0.5 and 1 μg, respectively. Tau protein, concentration varying from 0 to 10 μM, was mixed with microtubules at constant total MT concentration of 1.62 μM tubulin dimers. Bound tau was separated from free tau by centrifugation and fractionated on the SDS-PAGE lane 6–15. B) Two representative curves plotting the concentration of bound tau versus tau free in solution (● wild-type tau, ○ 7-Phos tau). The amount of bound tau was determined by the intensity of tau band on SDS-PAGE. The data were fit to a one site binding equation. K_d and n were

determined for each of three independent repetitions of the binding curves for each protein and shown in panels C and D, respectively. All data are presented as the average of three independent determinations of K_d and n ± s.d. (n=3). Values that were significantly different from wild-type values at $P < 0.05$ (*) and $P < 0.01$ (**) were determined by *t* test.

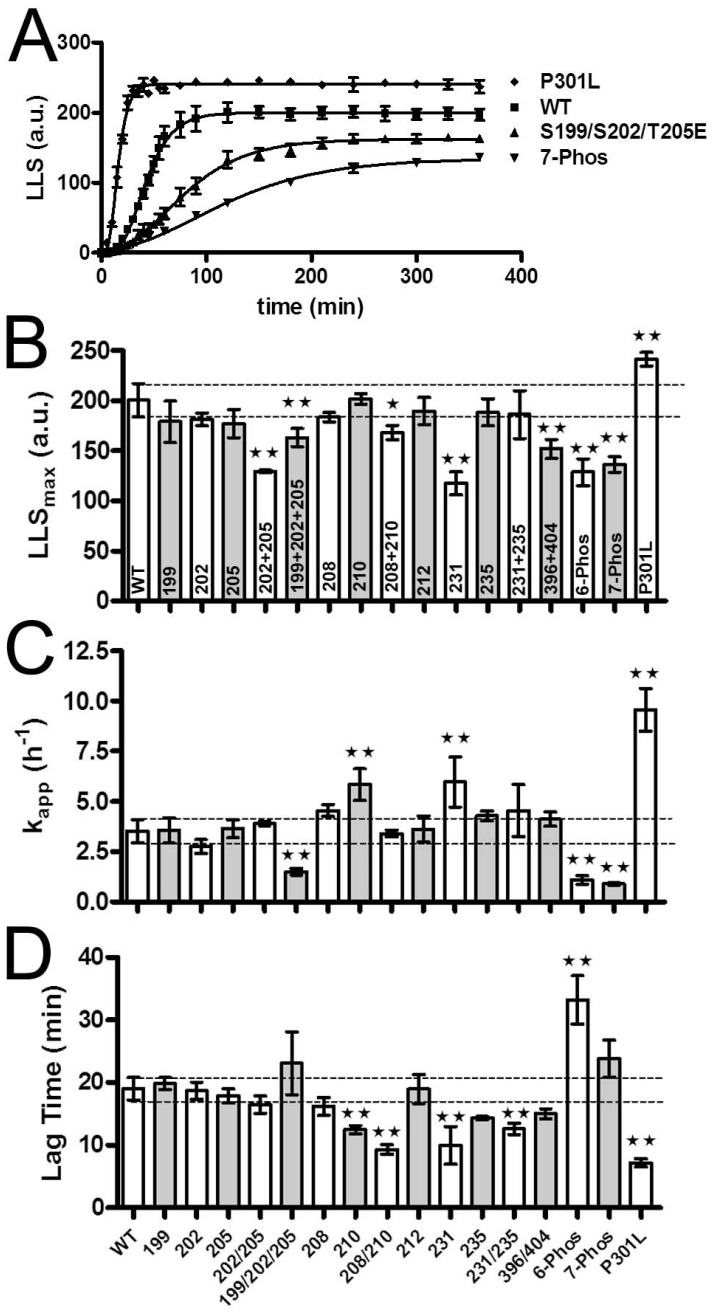

Figure 3. Kinetics of ARA induction of tau polymerization

The kinetics of wild-type and mutant tau polymerization at 2 μM protein and 75 μM ARA inducer were monitored by laser light scattering. A) Four representative averaged curves of the amount of light scattering (LLS) at the times indicated are shown for ■ wild-type; ▲ S199/S202/T205E, ▼ 7-Phos, and ◆ P301L. Each experimental data set was fit to a Gompertz function. LLS_{max}, k_{app} and lag time were determined from the equation as described in Materials and Methods and are shown in panels B, C and D respectively. All data are presented as averaged values ± s.d. from the three independent data sets. Values that were significantly different from wild-type values at $P < 0.05$ (*) and $P < 0.01$ (**) were determined by one-way

ANOVA analysis of variance with Dunnett's multiple comparison post-test using wild type as the control column.

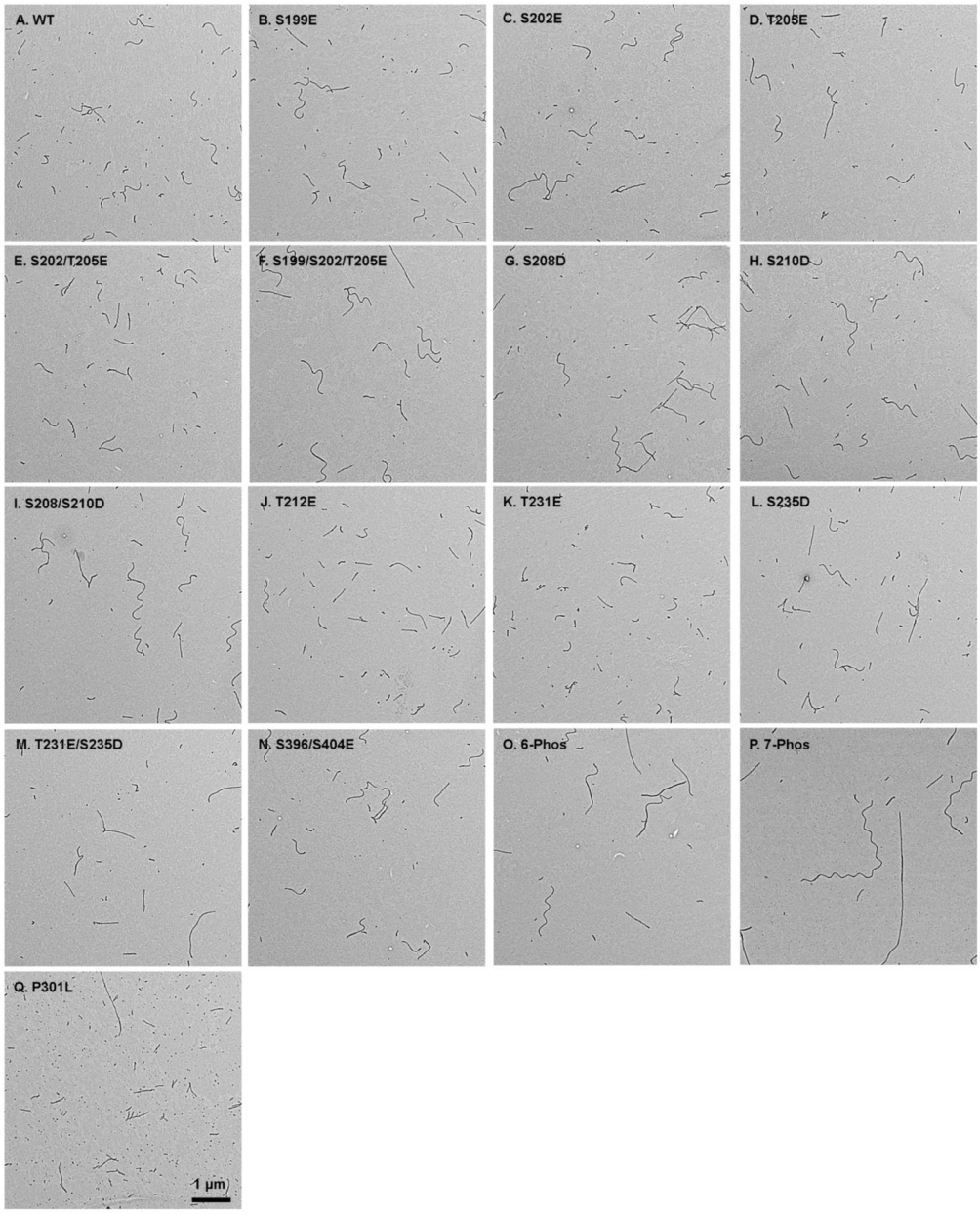

Figure 4. TEM analysis of polymerization at final concentration of 2 μM tau protein and 75 μM ARA inducer

The polymerization of wild-type and mutant tau at 2 μM protein and 75 μM ARA inducer were viewed by TEM after 20 hr incubation at room temperature. Representative micrographs are shown. A) wt, B) S199E, C) S202E, D) T205E, E) S202/T205E, F) S199/S202/T205E, G) S208D, H) S210D, I) S208/S210D, J) T212E, K) T231E, L) S235D, M) T231E/S235D, N) S396/S404E, O) 6-Phos, P) 7-Phos and Q) P301L. Scale bar in Q) represents 500 nm and is applicable to all images.

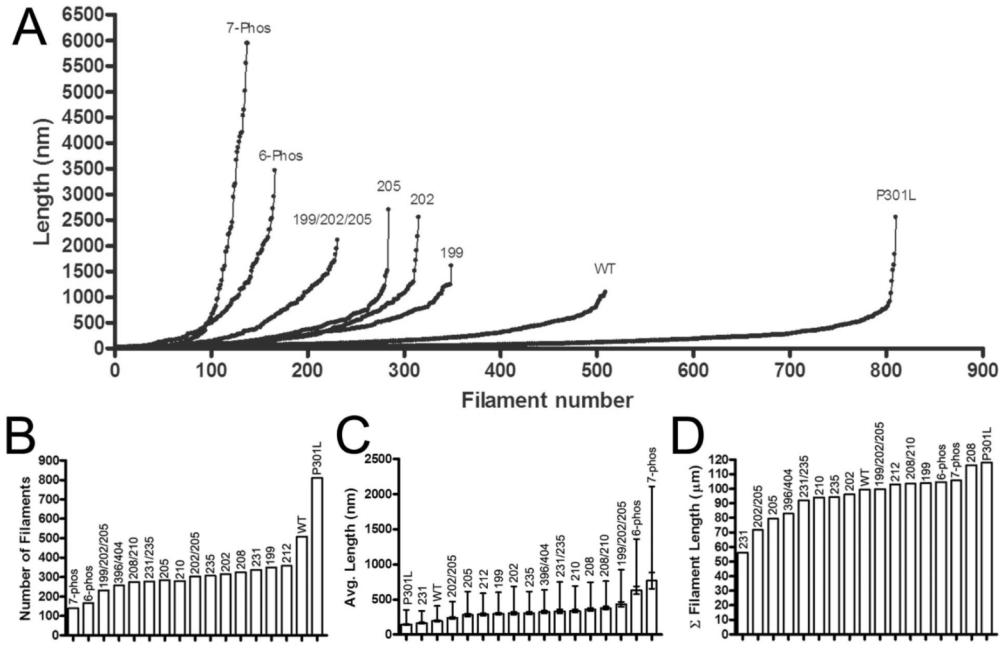

Figure 5. Filament distribution of polymerization at final concentration of 2 μM tau protein and 75 μM ARA inducer

The polymerization of wild-type and mutant tau at 2 μM protein and 75 μM ARA inducer were viewed by TEM after 20 hr incubation at room temperature. Resulting filament lengths were measured using Optimas image analysis software. Six 36 μm^2 fields were analyzed for each protein. A) The filament lengths were combined into a single data set and ranked from shortest to longest. Each individual filament length was plotted against its corresponding rank for each protein. Several examples are shown and are individually labeled on the graph. The distributions for S210D, S208/S210D, T231E/S235D and S396/S404E were similar to that of T205E. The distributions for S202/T205, S208D and S235D were similar to S202E. The distributions for T212E and T231E were similar to S199E. B) The total number of filaments observed in six 36 μm^2 fields are shown in ranked order from least to greatest. Each bar is individually labeled on the graph. C) The average length of the filaments observed in six 36 μm^2 fields are shown in ranked order from least to greatest. Each bar is individually labeled on the graph. Values are shown as averages ± s.d. (error bars above only) and ± s.e.m. (bars above and below). D) The sum of all filament lengths from six 36 μm^2 fields are shown in ranked order from least to greatest. Each bar is individually labeled on the graph.

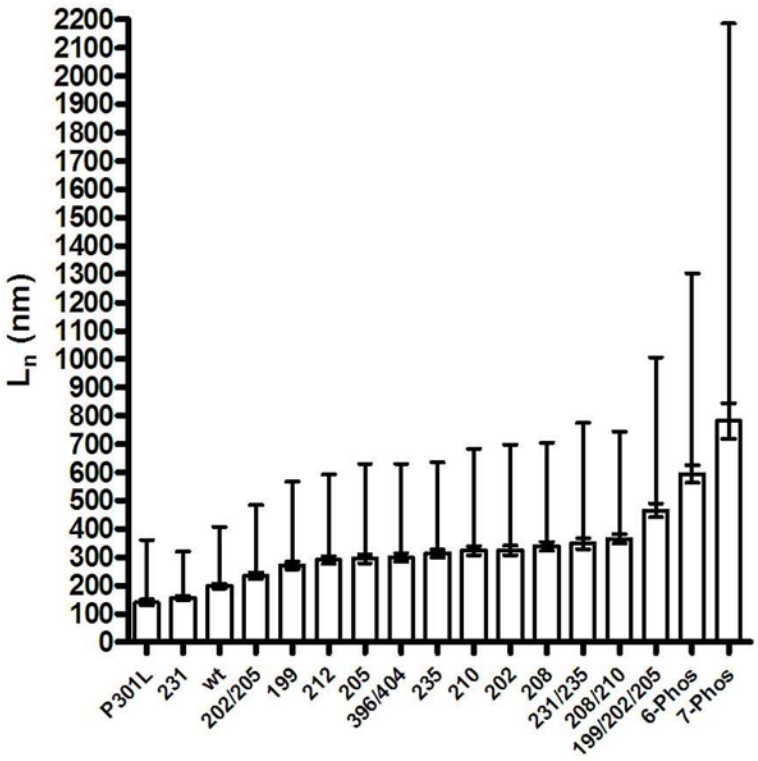

Figure 6. Pseudo-phosphorylation mutants form longer filaments than wild type tau

Wild-type and mutant tau protein (2 μM) were incubated in polymerization buffer with 75 μM ARA for 20 hr. Resulting filament lengths for 500 filaments were measured using Optimas image analysis software. The number-average length ± s.d. (error bars above) and ± s.e.m. (error bars above and below) for each protein was ranked by their average length and are labeled on the x-axis.

Table 1

Summary of effects of pseudophosphorylation on tau function compared to wild type.[a]

		Microtubule binding		Kinetics of polymerization			EM[g]	
Protein	SDS band shift	Kd[b]	n[c]	LLS_{max}[d]	k_{app}[e]	Lag time[f]	Avg L[h]	C_σ[i]
WT	no	0.20 ± 0.04	0.54 ± 0.08	200 ± 16	3.5 ± 0.6	19.0 ± 1.8	198	1.06
S199E							271	1.09
S202E							325	1.15
S208D							339	1.08
T212E		▲					291	1.04
T205E		▲					295	1.14
S235D		▲					314	1.02
231,235		▲				▼▼	348	1.23
S210D		▲▲			▲▲	▼▼	323	1.11
208,210		▲▲		▲		▼▼	365	1.04
396,404	▲	▲		▼▼			300	1.10
202,205		▲▲	▲	▼▼			235	1.07
T231E		▲		▼▼	▲▲	▼▼	156	1.05
199,202,205	▲	▲▲		▼▼	▼▼		466	1.16
7-Phos	▲	▲		▼▼	▼▼		781	1.80
6-Phos	▲	▲		▼▼	▼▼	▲▲	594	1.19
P301L		▲		▲▲	▲▲	▼▼	141	1.58

[a] Pseudophosphorylation variants are ranked by number of significant changes as compared to wild type. Triangles represent increases (▲) or decreases (▼) in values as compared to wild type. A single triangle represents $P > 0.05$ and two triangles represent $P > 0.01$. The number of triangles does not represent the magnitude of changes.

[b] Kd – Dissociation constant (μM ± s.d.)

[c] n – Maximal level of tau binding per tubulin molecule ([tau]/[tubulin])

[d] LLS_{max} – Maximum amount of right angle laser light scattering at ~ 20 h polymerization in arbitrary units ± s.d.

[e] k_{app} – Proportional growth rate of filaments in units of h^{-1} ± s.d.

[f] Lag Time – Approximate time (in minutes) before significant polymerization was detected ± s.d.

[g] EM – Electron microscopy

[h] Avg L – Number-average length of filaments in nm determined by measuring the lengths of 500 filaments ± standard deviation.

[i] C_σ – Coefficient of variation is equal to the mean divided by the standard deviation. For exponential length distributions, the average length is expected to be approximately equal to the standard deviation (46), or a C_σ of ~ 1.0..